



Composition of the Venus mesosphere measured by Solar Occultation at Infrared on board Venus Express

A.C. Vandaele, M. de Mazière, R. Drummond, A. Mahieux, E. Neefs, V. Wilquet, O. Korablev, A. Fedorova, D. Belyaev, Franck Montmessin, et al.

► To cite this version:

A.C. Vandaele, M. de Mazière, R. Drummond, A. Mahieux, E. Neefs, et al.. Composition of the Venus mesosphere measured by Solar Occultation at Infrared on board Venus Express. *Journal of Geophysical Research. Planets*, 2008, 113 (E5), pp.E00B23. 10.1029/2008JE003140 . hal-00349440

HAL Id: hal-00349440

<https://hal.science/hal-00349440>

Submitted on 9 Mar 2016

HAL is a multi-disciplinary open access archive for the deposit and dissemination of scientific research documents, whether they are published or not. The documents may come from teaching and research institutions in France or abroad, or from public or private research centers.

L'archive ouverte pluridisciplinaire **HAL**, est destinée au dépôt et à la diffusion de documents scientifiques de niveau recherche, publiés ou non, émanant des établissements d'enseignement et de recherche français ou étrangers, des laboratoires publics ou privés.

Composition of the Venus mesosphere measured by Solar Occultation at Infrared on board Venus Express

A. C. Vandaele,¹ M. De Mazière,¹ R. Drummond,¹ A. Mahieux,¹ E. Neefs,¹
V. Wilquet,¹ O. Korabiev,² A. Fedorova,² D. Belyaev,² F. Montmessin,^{3,4}
and J.-L. Bertaux^{3,4}

Received 14 March 2008; revised 20 June 2008; accepted 4 September 2008; published 27 December 2008.

[1] Solar Occultation at Infrared (SOIR), which is a part of the Spectroscopy for Investigation of Characteristics of the Atmosphere of Venus (SPICAV) instrument on board Venus Express, combines an echelle-grating spectrometer with an acoustooptical tunable filter. It performs solar occultation measurements in the IR region at a high spectral resolution better than all previously flown planetary spectrometers. The wavelength range probed allows for a detailed chemical inventory of the Venus atmosphere above the cloud layer, with an emphasis on the vertical distribution of the gases. A general description of the retrieval technique is given and is illustrated by some results obtained for CO₂ and for a series of minor constituents, such as H₂O, HDO, CO, HCl, and HF. Detection limits for previously undetected species will also be discussed.

Citation: Vandaele, A. C., et al. (2008), Composition of the Venus mesosphere measured by Solar Occultation at Infrared on board Venus Express, *J. Geophys. Res.*, 113, E00B23, doi:10.1029/2008JE003140.

1. Introduction

[2] Venus is a very warm and dry planet with a dense atmosphere composed mainly of carbon dioxide (CO₂, 96.5%) and Nitrogen (N₂, 3.5%). Chemically active species, such as sulfuric bearing gases (OCS and SO₂) and halides (HCl and HF) have already been reported (see *de Bergh et al.* [2006] for a general review on the composition of the atmosphere of Venus below 100 km altitude). Measurements have been performed essentially in the mesosphere below 100 km and below the clouds. Information about minor atmospheric constituents, their concentration, reactions, sources and sinks is incomplete, as for example only scarce measurements have been performed above 100 km altitude. In particular, photochemical models of the middle atmosphere would benefit from abundance measurements of Cl-bearing gases.

[3] The Solar Occultation at Infrared (SOIR) spectrometer is an extension mounted on top of the Spectroscopy for Investigation of Characteristics of the Atmosphere of Venus (SPICAV) instrument [Bertaux et al., 2007a]. SPICAV/SOIR is one of the seven instruments on board Venus Express, a planetary mission of the European Space Agency (ESA) that was launched in November 2005 and inserted into orbit around Venus in April 2006 [Titov et al., 2006].

[4] SOIR [Nevejans et al., 2006] is designed to measure at high resolution (0.15 cm⁻¹) the atmospheric transmission in the IR (2.2–4.3 μm) using solar occultations. This technique allows for the derivation of unique information about the vertical structure and composition of the Venus mesosphere. SOIR is the first high-resolution NIR spectrometer on board a spacecraft investigating the Venusian atmosphere and it enables a sensitive search for new minor species from the top of the clouds up to about 125 km of altitude.

2. Description of the Instrument

[5] The instrument has already been extensively described elsewhere [Bertaux et al., 2007a; Mahieux et al., 2008; Nevejans et al., 2006] and will only be briefly described here. SOIR is an echelle-grating spectrometer operating in the IR, combined with an acoustooptic tunable filter (AOTF) for the selection of the diffraction-grating orders. The free spectral range (FSR) of the echelle spectrometer, i.e., the spectral interval in which there is no interference or superposition of light from adjacent orders equals 22.38 cm⁻¹, whereas the bandwidth of the AOTF was originally designed to be 20 cm⁻¹, as measured on ground before launch [Nevejans et al., 2006]. The real measured bandwidth of SOIR is ~24 cm⁻¹ [Mahieux et al., 2008], creating some order leakage on the detector. The wave number domain that can be investigated by the SOIR instrument extends from 2256 to 4369 cm⁻¹, and is divided into 94 smaller ranges corresponding to the different orders (from 101 to 194). The detector width for orders 101 to 122 is smaller than the FSR of 22.38 cm⁻¹ and hence the detector will miss part of the spectrum. For orders 123 to

¹Belgian Institute for Space Aeronomy, Brussels, Belgium.

²Space Research Institute, Moscow, Russia.

³Service d'Aéronomie du CNRS, Verrières-le-Buisson, France.

⁴Institut Pierre Simon Laplace, Université de Versailles-Saint-Quentin, Saint Quentin en Yvelines, France.

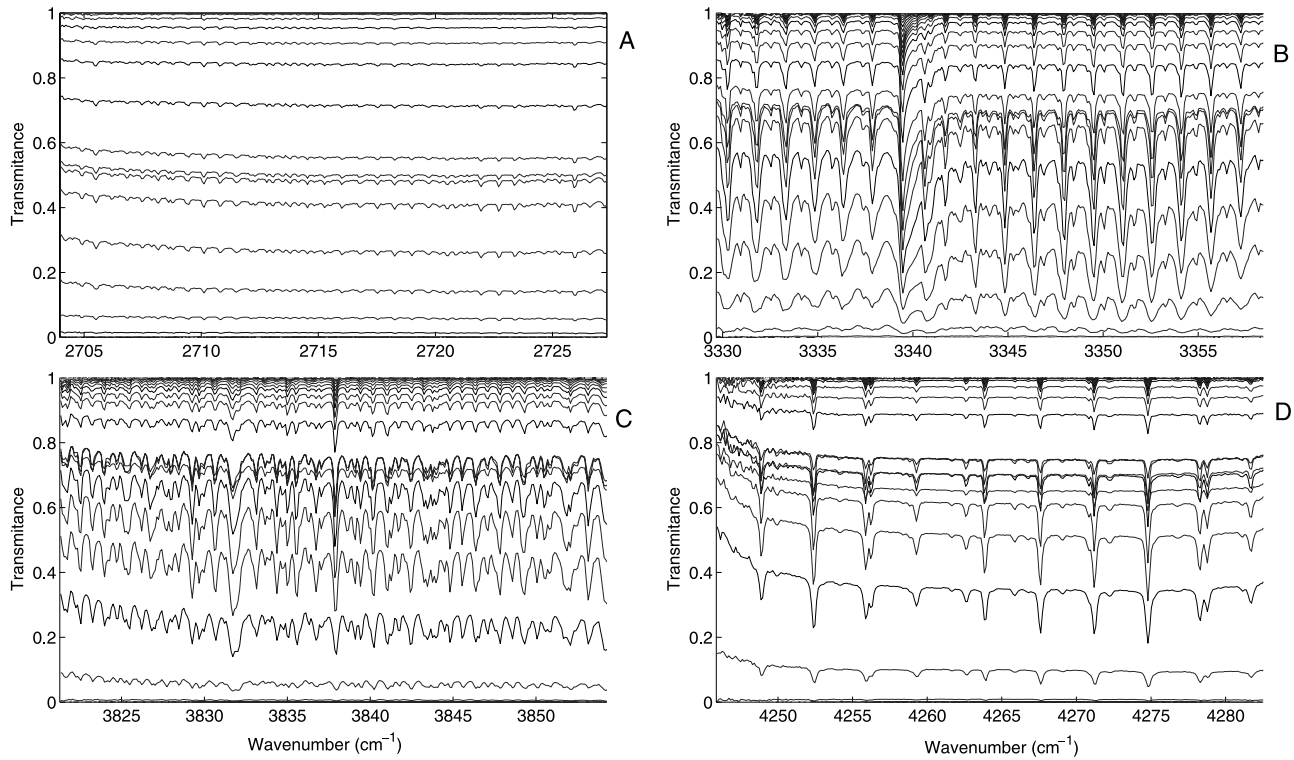


Figure 1. Example of spectra obtained during one occultation (sunset 15 April 2007). Each transmittance is obtained by making the ratio of the solar spectrum seen through the Venus atmosphere to the unattenuated solar spectrum measured above the atmosphere. The selection of a spectral interval is achieved through the acoustooptic tunable (AOT) filter, tuned in this case to (a) 15809 kHz for diffraction order 121, (b) 19869 kHz for diffraction order 149, (c) 23031 kHz for diffraction order 171, and (d) 25742 kHz for diffraction order 190. In these particular ranges of wave number, the main absorption lines are from HDO (Figure 1a), CO₂ (Figure 1b), H₂O (Figure 1c), and CO (Figure 1d).

194 the inverse happens: the detector width is equal to or larger than the FSR and the detector will not be completely covered by the selected order.

[6] The SOIR detector has 320 columns along the wave number axis and 256 rows along the spatial axis. The slit is projected on 32 fixed rows only. Since, owing to imposed telemetry limitations, only a data volume equivalent to 8 rows of 320 pixels can be retrieved per second, one is forced to bin the rows in eight groups of four rows, provided only one order (or AOTF frequency setting) is used during a given second. It is however possible to select up to four different orders (not necessarily sequential) per second, allowing us to gather a more versatile set of absorption lines. This reduces the maximum measurement time per order to 250 ms and implies that only 2 larger bins of 16 rows will be used if the complete slit height has to be covered. Later, the binning was changed to 2 bins of 12 rows because the outside rows of the illuminated part of the detector received a lower signal, because that part of the slit was too close to the edge of the Sun [Mahieux *et al.*, 2008]. Background measurements are subtracted onboard from the measurements themselves.

[7] Raw spectra, registered by SOIR and transmitted to Earth, need dedicated processing in order to upgrade them to a calibrated data set. This involves detector nonlinearity correction, spectral calibration and division by a reference solar spectrum. Ideally, the reference spectrum that is taken

outside the atmosphere would be measured with an identical relative slit position with respect to the solar disk. Attitude drift of the spacecraft, however, makes the slit float which results in a gradual linear change of the intensity. This effect is also corrected for Mahieux *et al.* [2008].

[8] A SOIR occultation observation can be taken either at sunset or sunrise. In the case of a sunset, the measurement cycle is started well before the instrument's line of sight to the Sun intersects with the top layers of the atmosphere, and reference spectra are recorded (at a rate of 1 spectrum s⁻¹). Once the top of the atmosphere is reached, solar light is absorbed and the intensity of the recorded signal starts to decrease until the Sun gets so flattened by refraction that the spectrometer slit moves out of the refracted solar disk. One of the main advantages of solar occultations is that it is a self-calibrated technique in terms of transmission: dividing a spectrum obtained during the occultation by a reference solar spectrum recorded outside the atmosphere removes the solar signature and leaves a transmittance containing only information about the composition of the Venus atmosphere. The reference spectrum is in fact defined by selecting spectra recorded within the 40 s before the level at 220 km is reached.

[9] Figure 1 gives an example of the evolution of the spectra through one occultation (sunset 15 April 2007) in the orders 121, 149, 171, and 190 corresponding to the 2725–2750, 3330–3357, 3820–3855, and 4245–4283 cm⁻¹

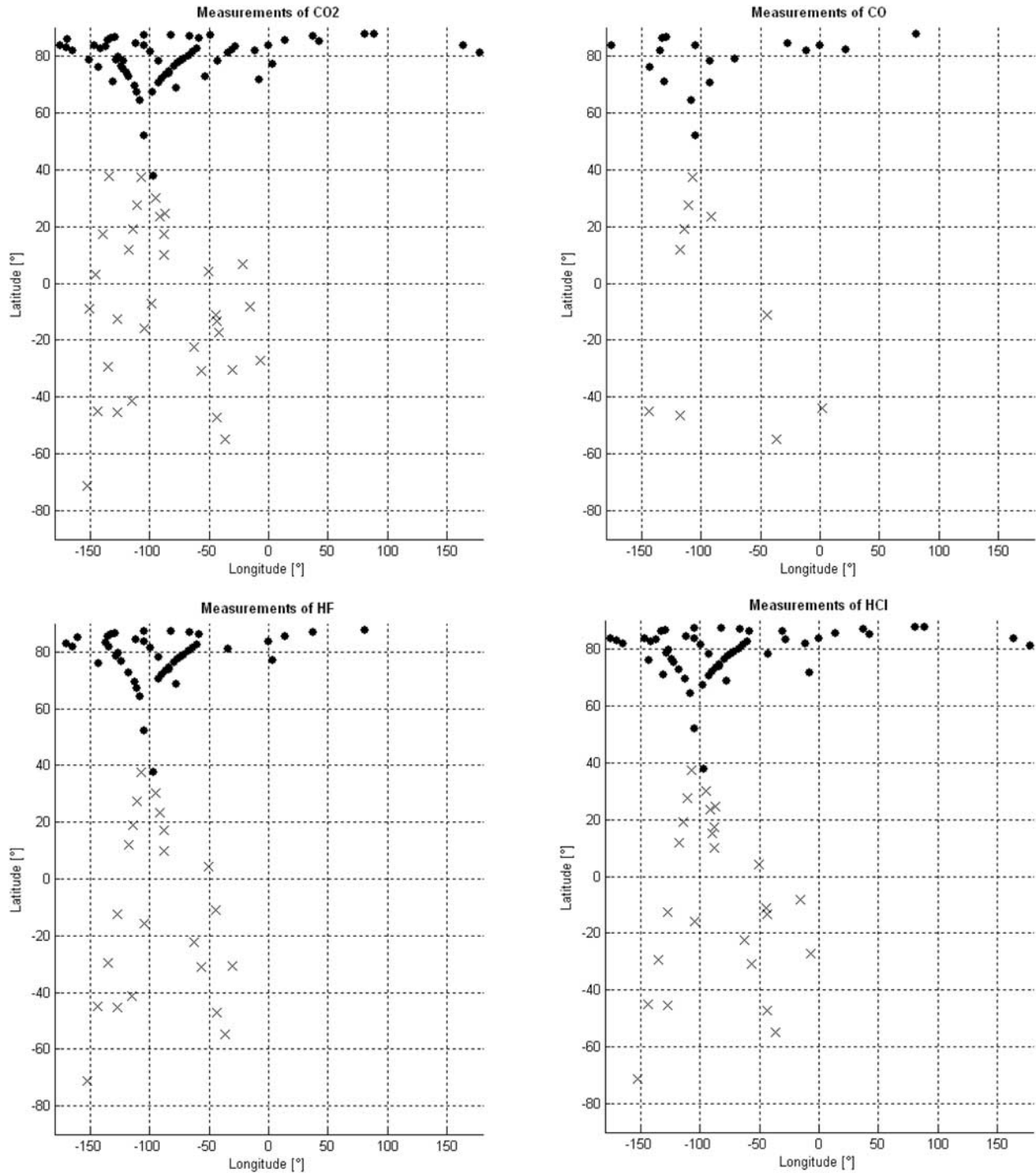


Figure 2. Latitudinal distribution of measurements of (a) CO_2 , (b) CO , (c) HF , and (d) HCl . Dots represent measurements performed when Venus Express is separated from limb at 65 km tangent height by less than 5000 km and crosses when this distance is larger. In the latter case, the vertical resolution is coarser. Only measurements corresponding to the smallest distances have been considered in this study. Most of those correspond to north polar air masses.

ranges, respectively. These transmittances show the characteristic behavior observed on all occultation series measured by SOIR. At the beginning of the series, the light path does not cross the atmosphere. No absorption signatures are present and transmittances are equal to unity. As the Sun

sets, the light path goes deeper and deeper into the atmosphere, and two absorption processes take place: the overall signal decreases owing to extinction by aerosols and absorption signatures appear. At the end of the observation, no light is captured anymore when the Sun disappears behind

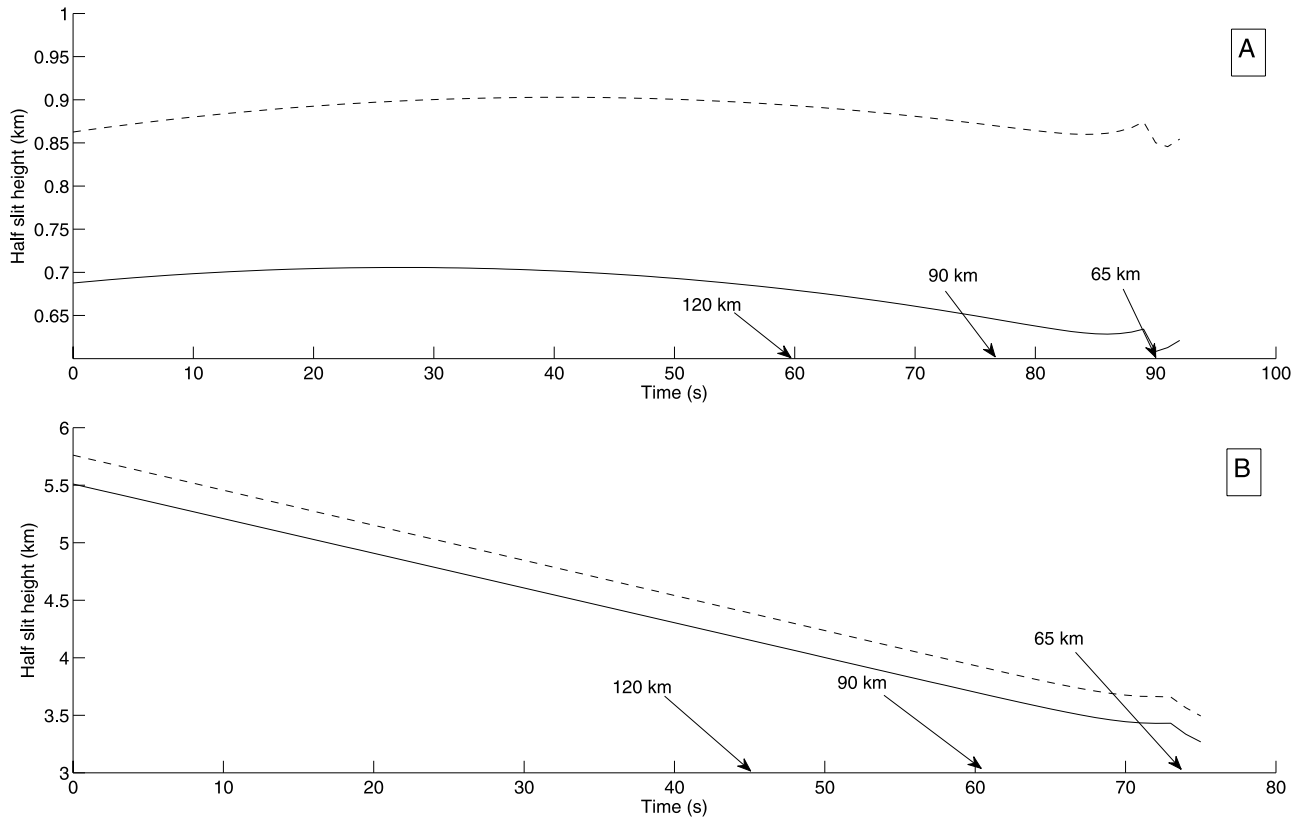


Figure 3. Typical examples of the vertical resolution for different types of orbits. The geometry of the orbit defines the field of view (instantaneous range of altitude encompassed by the instrument entrance slit taken at the beginning of the measurement, solid line) and the vertical resolution (dashed line). This corresponds to the portion of atmosphere sounded during one measurement, thus 250 ms. It highly depends on the distance from the planet and the velocity of Venus Express (VEX). Figures 3a and 3b show the vertical resolution and the field of view during orbits 223 (30 November 2006; distance to the limb at 65 km tangent height is 2000 km; 81°N) and 332 (19 March 2007; distance to the limb is 11198 km; 4°N) as a function of time.

the cloud deck or moves out of SOIR's field of view owing to diffraction. The structures seen in the spectra of Figure 1 are mainly attributed to HDO (Figure 1a), CO₂ (Figure 1b), H₂O (Figure 1c), and CO (Figure 1d). From Figure 1, it can also be seen that in general, the SOIR spectra contain information on the Venus atmosphere between 65 and 110 km for molecules such as HDO or HCl. For H₂O and CO signatures are still observable up to 130 km altitude and CO₂ features are seen up to 125–130 km [Bertaux *et al.*, 2007b; Wilquet *et al.*, 2007].

[10] Most of the measurements of SOIR occur at high northern latitude because of the shape of the orbit with its pericenter located at about 250 km above the northern pole and its apocenter at about 65,000 km. When solar occultation occurs, a sunset or a sunrise can be observed. When the satellite is close to the planet the vertical resolution is less than 1 km. Measurements correspond to latitudes ranging from 60° to 90°N. When the satellite is located far from Venus, measurements have a poorer vertical resolution and occur at lower latitudes, typically from 70°S to 60°N. Figure 2 illustrates the latitudes and longitudes, corresponding to the tangent altitude of 65 km, of the measurements yielding information on CO₂, CO, HCl, and HF. We have distinguished two types of geometries, when the distance between

Venus Express (VEX) to the limb (at 65 km tangent height) is less than 5000 km (dots), and when it is larger (crosses). Figure 2 will be discussed in more detail in section 4, where results for each species will be described individually.

[11] We define the vertical resolution at the tangent point as the total altitude range scanned during one measurement. Because the slit is not always parallel to the limb, but rotating slightly, and because the measurement lasts for 250 ms, this vertical resolution may vary between 100 m and several kilometers in the worst cases. Another variable is the field of view, which is defined as the instantaneous height encompassed by the instrument slit at the beginning of the measurement. This parameter always gives a lower limit to the vertical resolution. The vertical resolution is mainly a function of the distance of the satellite to the planet. The distance of the spacecraft to the planet and the velocity of the spacecraft influence the vertical resolution in the following ways: (1) the further the spacecraft is from the limb, the larger the size of the instantaneous height measured in the atmosphere; (2) the velocity of the spacecraft projected at the limb on the atmospheric local vertical depends on the position of the spacecraft on its orbit around Venus at the moment of the occultation.

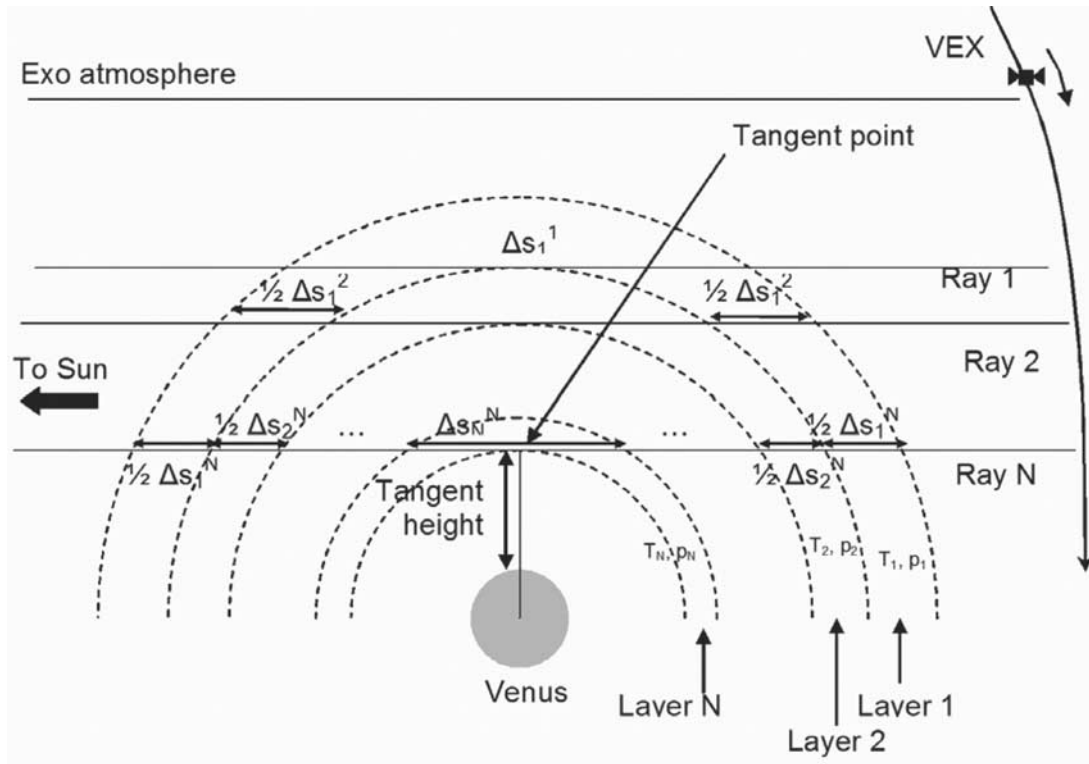


Figure 4. Geometry of solar occultation measurements and definition of the onion-peeling method.

[12] Figure 3 shows the variation of the field of view and vertical resolution as a function of time of orbit 223 (30 November 2006; distance to the limb at 65 km tangent height is 2000 km; 81°N) and 332 (19 March 2007; distance to the limb is 11,198 km; 4°N). During orbit 332, the spacecraft was far away from the planet which implies a large atmospheric height seen by the instrument slit. The field of view and vertical resolution are very similar because the Sun is rising almost vertically in the atmosphere and the velocity of the spacecraft is not too high (the spacecraft is almost at the equator). During orbit 223, spacecraft is close to the planet and the instantaneous height of the sounded atmosphere is much smaller. The velocity is higher, because the spacecraft is almost at pericenter (87°N). For the reasons explained just above, we will limit the retrieval to spectra obtained under favorable conditions, i.e., corresponding to low distance between VEX and the limb at 65 km tangent height (<5000 km) and with vertical resolution of less than 2 km. As can be inferred from Figure 2, this condition limits the selection to regions near the north pole, with latitudes above 60°N.

3. Description of the Retrieval Technique

[13] The retrieval technique is based on the onion peeling method, illustrated in Figure 4. The atmosphere is treated as an onion-like composite of spherical layers, in which the temperature, pressure, and mixing ratios of the constituents are held constant.

3.1. Forward Model

[14] Quantitative analysis of the recorded spectra needs first the calculation of synthetic spectra through a forward

model based on the fundamental knowledge of the optical properties of the atmosphere. In the forward model, SOIR spectra are simulated using a line-by-line (LBL) code developed initially for Earth exploration [Vandaele *et al.*, 2006] and adapted for the conditions on Venus. The general equation describing radiative transfer through the atmosphere can be written as

$$I(\nu) = I_0(\nu)e^{-\tau(\nu,0,s_{obs})} + \int_0^{s_{obs}} B(\nu, T(s))\alpha(\nu, s)e^{-\tau(\nu,0,s)} ds \quad (1)$$

where I_0 represents the light intensity of the source (here the Sun) placed at the starting point of the raypath situated at the distance s_{obs} from the observer, $\alpha(\nu, s)$ is the absorption coefficient, $B(\nu, T)$ is the Planck function, and

$$\tau(\nu, s_1, s_2) = \int_{s_1}^{s_2} \alpha(\nu, s) ds \quad (2)$$

is the optical depth along the path between the points s_1 and s_2 . In solar occultation, the second term is often negligible with respect to the Sun intensity. The optical depths τ of the absorbing constituents along the line of sight (see Figure 4) are calculated at high resolution in each layer considering the temperature and pressure determined by the ray-tracing procedure:

$$\tau(\varphi, \nu) = \int_s \alpha(P(s), T(s), \nu) ds \quad (3)$$

where τ is a function of wave number and depends on the tangent height. This, in turn, depends on the solar zenith angle φ and on the atmospheric refraction characteristics, which, on Venus, are far from negligible. Starting from known temperature and pressure vertical profiles, the ray-tracing calculations are carried out on a finer grid (with a 200 m step) and the final results, i.e., the effective temperature and pressure in each layer as well as the effective densities, are obtained using the Curtis-Godson approximations [Goody and Yung, 1995]. In this work, we have used temperature and pressure vertical profiles from the VIRA model for altitudes up to 100 km [Seiff et al., 1985]. For higher altitudes (from 140 km and upward), data were taken from the model of Hedin et al. [1983] as suggested by Mueller-Wodarg and Tingle [2008]. The transition between the two data sets was performed by spline interpolating the temperature and reconstructing the pressure through the hydrostatic law. In the following we will refer to this composite model as the VENUSREF model.

[15] The extinction coefficient $\alpha(P, T, \nu)$ is a function of the temperature and pressure prevailing at altitude z . It represents all absorption processes, including Rayleigh α_R and aerosol α_A extinction and absorption by molecular species:

$$\alpha(P(z), T(z), \nu) = \alpha_R(z, \nu) + \alpha_A(z, \nu) + \sum_{i=1}^M \sigma_i(P(z), T(z), \nu) N_i(z) \quad (4)$$

where M is the number of absorbing species, σ_i and N_i are the absorption cross section and number density of species i . The contribution of the aerosols will be further described and discussed in a later paper (V. Wilquet et al., Characterization of the upper Venusian haze from UV to mid-IR by SPICAV/SOIR on Venus Express, submitted to *Journal of Geophysical Research*, 2008). The contribution of each species is determined using a line-by-line model based on a line catalog specific to Venus, as explained later (see section 3.2). The absorption coefficient k_{ij} (cm^2 molecule $^{-1}$) for a particular line j of species i is given as

$$k_{ij}(\nu, T, P, p_i) = S_{ij}(T) \times \phi(\nu, \nu_{ij}, T, P, p_i) \quad (5)$$

where $\phi(\dots)$ is a normalized line shape. The intensity $S_{ij}(T)$ exhibits a temperature dependence which can be described as

$$S_{ij}(T) = S_{ij}(T_0) \frac{Q_i(T_0)}{Q_i(T)} e^{\left(c_2 E_j \left(\frac{1}{T_0} - \frac{1}{T}\right)\right)} \frac{1 - e^{-c_2 \nu_{ij}/T}}{1 - e^{-c_2 \nu_{ij}/T_0}} \quad (6)$$

where c_2 is the second Planck constant hc/k_B (1.4387 cm K), with h the Planck constant, k_B the Boltzmann constant, and c the speed of light, $\nu_{0,j}$ is the central wave number of the j th transition, E_j is the energy of the lower state (cm^{-1}), and $S_{ij}(T_0)$ is the intensity at the reference temperature T_0 (cm^{-1} molecule $^{-1}$ cm^2). $Q(T)$ and $Q(T_0)$ are the total partition functions under local thermodynamic equilibrium condi-

tions, at temperature T and T_0 , respectively. These functions describe the temperature dependence of the line intensity of the transition. They are approximated by

$$Q(T) = a_0 + a_1 T + a_2 T^2 + a_3 T^3 \quad (7)$$

where a_0, a_1, a_2 , and a_3 are tabulated coefficients [Gamache et al., 1990]. ASIMUT allows the user to select between different line profiles, the Voigt profile being the default. In the case of the H_2O and CO_2 molecules, sub- and super-Lorentzian line profiles have been observed [Clough et al., 1989; Pollack et al., 1993], which are characterized by a symmetric or asymmetric χ function:

$$\phi_\chi(\nu) = \chi(\nu) \times \phi_L(\nu, P, T) \quad (8)$$

This correction factor has been introduced to take into account the fact that far from the line center, the line displays marked deviations from the Lorentzian behavior ϕ_L . Typically, CO_2 displays a sub-Lorentzian behavior (the opacity far from the line center is less than that predicted by a Lorentzian profile) whereas H_2O shows a super-Lorentzian behavior. The χ function is usually defined on large spectral intervals.

[16] The spectral grid, on which the profile must be determined, must be fine enough so that the narrowest line be adequately represented. In the upper atmosphere, the Doppler width is the limiting factor for selecting an adequate sampling value. As Doppler width depends on temperature, it varies with altitude; the line profile must therefore be sampled with different steps as the altitude varies. ASIMUT determines for each layer, of temperature T and pressure P , the optimized sampling step as

$$\Delta\nu(P, T) = \frac{1}{4} \sqrt{\alpha_D^2(T) + \alpha_L^2(P, T)} \quad (9)$$

with α_D the Doppler width obtained for a molecule of mass 20.0, and α_L the Lorentzian width obtained for a molecule characterized by no self-broadening, a foreign broadening of $0.04 \text{ cm}^{-1} \text{ atm}^{-1}$, and a temperature coefficient of 0.5. However, for some particular temperature and pressure conditions, this sampling step might be too large compared to the desired final resolution. In that case, the sampling is set to the value of final resolution/15. LBL calculations often require the computation of a large number of line shapes over large to very large spectral intervals. The number of points might then become prohibitive. However, it can be observed that the line profile changes slower at a distance from the line center than it does near the center. The solution implemented in ASIMUT is the use of a nonuniform grid: near the center of the line, the optimized step derived with the help of equation (9) is used; the step is then progressively enlarged as one goes away from the center. Our algorithm is based on the study of Fomin [1995], which splits the spectral grid in a series of subintervals. Let us assume that the line shape must be calculated on the interval D , for which a value of 25 cm^{-1} is considered sufficiently large for most of the simulations, except when applying a χ factor. The cutoff value D is then determined by the interval on which this function is given.

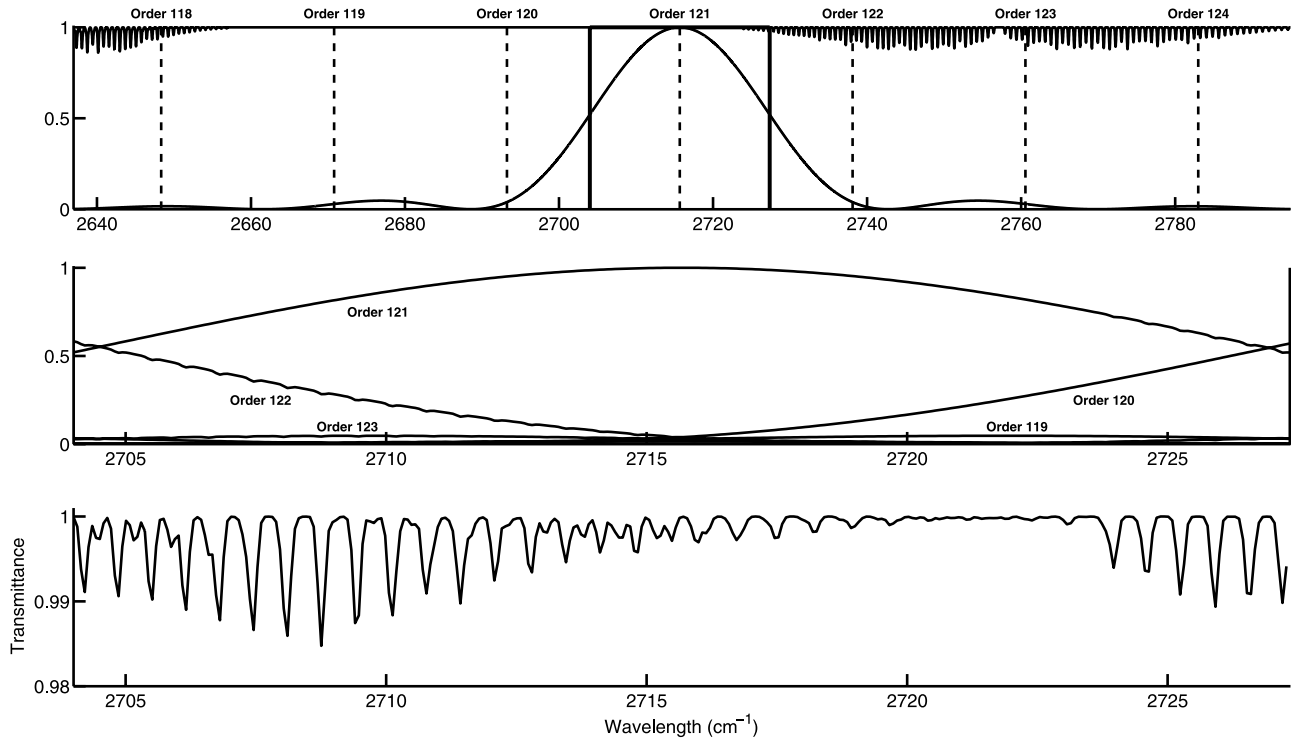


Figure 5. Description of the order overlap occurring in the instrument owing to the combined presence of the AOTF filter and the different diffraction orders of the echelle grating. In the top, a simulated spectrum is shown containing only CO₂. It spans several diffraction orders whose limits are also indicated. This spectrum is first filtered by the AOTF, and only the portion under the filter bandwidth enters the spectrometer. Because this bandwidth is larger than the free spectral range (FSR) of the echelle spectrometer, more than one order of diffraction is transmitted. This is illustrated in the middle, where the contributions of the different orders are represented. Finally, in the bottom, the sum of all of these contributions is measured on the detector.

The limits of the center zone are defined by $[\nu - C, \nu + C]$ with $C = 2/3 (\alpha_D + \alpha_L)$, α_D and α_L being the Doppler and Lorentzian widths of the line. The grid is divided into $2L$ portions located at unequal intervals:

$$\begin{aligned}
 &[\nu - D, \nu - 2^{L-1}C], \dots, [\nu - 2^2C, \nu - 2C], [\nu - 2C, \nu - C], \\
 &\text{central zone, } [\nu + C, \nu + 2C], [\nu + 2C, \nu + 2^2C], \dots, \\
 &[\nu + 2^{L-1}C, \nu + D]
 \end{aligned} \quad (10)$$

The number of intervals is related to D and C through the following expression:

$$2^L \times C = D \quad (11)$$

In the central zone, the sampling is set to the optimized value determined with equation (9). Then in each subsequent interval, the sampling is doubled. This drastically reduces the number of points on which the line profile is calculated, without losing accuracy at the center of the line. At the end, the absorption line shape is interpolated to correspond to the sampling used for the determination of the optical depth (OD). The latter is chosen by considering the step asked for the radiance or transmission simulation and an oversampling factor either provided by the user or chosen such that the OD wave number step is a factor 10 lower than the final radiance step.

[17] Radiances are finally convolved by the instrumental function of the instrument, which is chosen to be a Gaussian, whose width varies between 0.13 and 0.25 cm⁻¹ depending on the spectral interval simulated [Mahieux et al., 2008].

[18] At this point, one must take into account the effect of the AOTF on the measured spectrum. As already noted, the filter has a bandwidth larger than the free spectral range of the echelle spectrometer, implying some order overlap on the detector. This is illustrated in Figure 5 where the contribution of four adjacent orders on top of the central one are considered. The incoming spectrum is represented in the Figure 5 (top), along with the position of the different orders of diffraction spanned by the AOTF filter bandwidth. The position of the maximum of the AOTF bandwidth is determined by the selected RF applied to the device. It is necessary to determine the best possible (AOTF frequency–wave number) calibration curve to increase the accuracy of the simulation. This is done through the careful analysis of specific measurements of some selected solar lines, whose positions are well known [Mahieux et al., 2008]. In the case illustrated here, the RF applied to the AOTF corresponds to the central order number 121. The entire signal received on the detector comes from the adjacent orders as no absorption is present in the incoming spectrum in the range of the central order of diffraction. The contribution coming from the noncentral orders is certainly not negligible and has to

be taken into account when simulating SOIR spectra. In general, we consider a total of 7 contributing orders to determine the final transmittance.

[19] The resulting transmittance is then interpolated to correspond to the wave number values of the observed spectrum. It is possible to fit a wave number shift between the observed and simulated transmittances to optimize the correspondence.

3.2. Spectroscopic Data Sets

[20] Spectroscopic data, i.e., line parameters, have been taken from the latest version of the HITRAN database [Rothman *et al.*, 2005]. However, broadening coefficients have been modified in order to take into account the presence of CO₂ as main buffer gas, whereas data reported in HITRAN are given for Earth-like air conditions.

[21] Sung and Varanasi [2005] reported CO₂-broadened half widths and CO₂-induced line shifts for the fundamental (1–0) of ¹²C¹⁶O at 201, 244, and 300 K, as well as for the first (2–0) overtone and the second (3–0) overtone bands at 298 K. We have considered their values for the lines in common with the HITRAN database. Those which are not reported by Sung and Varanasi have been corrected by a conversion factor air width (shift) to CO₂ width (shift) derived from the comparison of available common values. The temperature coefficient has been held constant for all lines ($n = 0.73$), as suggested by Sung and Varanasi.

[22] Toth and Darnton [1974] have performed measurements of the HCl line widths by CO₂ in the 1–0 and 2–0 bands of HCl. Their values have been taken for the lines in common with the HITRAN database. A correction similar to the one devised for CO was applied to the lines not reported by those authors.

[23] Air-broadening measurements performed by the Brussels-Reims group [Fally *et al.*, 2003; Jenouvrier *et al.*, 2007; Mérienne *et al.*, 2003] up to 25,000 cm^{−1} have revealed that there is a large vibrational dependence of the width for most of the H₂O transitions. This is also the case under a CO₂ rich atmosphere. Various attempts [Brown *et al.*, 2007; Gamache *et al.*, 1995] have tried to give simple relations between the quantum vibrational numbers and the width and shift of the lines. However, the spectrum of water is so complex that it is virtually impossible to obtain measured values for each band, reducing the validity of the proposed relations. A simplistic solution is to scale the broadening coefficients obtained with other perturbing gases, such as N₂ or air, although it has been pointed out by Brown *et al.* [2007] that “simple scaling of existing values of air- or nitrogen-broadened parameters will not achieve sufficiently reliable CO₂-broadened H₂O coefficients”, as these authors found considerable scatter of the ratio of CO₂ to air broadened width (from 0.95 to 3.07) around the mean value of 1.67. However, no data, neither experimental nor calculated, are available in the spectral region investigated by SOIR and the constant factor of 1.67 was applied to correct the air-broadening coefficient given in HITRAN. This value has to be compared to the value of 1.3 usually used in Venus studies [Pollack *et al.*, 1993].

3.3. Onion-Peeling Method

[24] The onion-peeling method was implemented to coherently treat a series of spectra recorded during one

occultation. In this method, one starts the analysis in the uppermost layer, i.e., with the first spectrum containing absorption structures due to the constituents of the atmosphere, deriving concentrations in that layer, and progressively goes deeper into the atmosphere taking into account the results from the layers above. Vertical profiles of several key species of the Venusian atmosphere have been obtained by applying this technique, as will be demonstrated hereafter.

[25] For the sake of clarity, we will consider in the following that the second right term in equation (1) is negligible. The observed transmittance Tr_1 corresponding to ray 1 passing through the uppermost layer (layer 1 in Figure 4) is then given by

$$Tr_1(\nu) = \exp[-\alpha_1(\nu)\Delta s_1^1] \quad (12)$$

where $\alpha_1(\nu)$ stands for $\alpha(T_1, P_1, \nu)$ determined using equation (4) and Δs_1^1 is the length of the raypath in layer 1 obtained by the ray-tracing procedure already explained. In this expression, the only unknowns are the concentration N_i of each species and the aerosol loading in layer 1, which are retrieved from the analysis of this first layer. Transmittance observed for ray 2 will result from the combination of the absorption of light in layer 1 (Δs_1^2) and layer 2 (Δs_2^2). If we moreover consider the atmosphere as spherical and homogeneous, we can further write

$$Tr_2(\nu) = \exp[-\alpha_2(\nu)\Delta s_2^2 - \alpha_1(\nu)\Delta s_1^2] \quad (13)$$

in which the only unknowns are the concentration N_i of each species and the aerosol loading in layer 2. By going down progressively, the vertical profiles of the interacting species can be derived.

4. Results

[26] In this section, we will present some results of our analysis concerning the various species unambiguously detected with SOIR. CO₂, being the most prominent absorber in the IR region, can be probed in different spectral regions. Combining different diffraction orders in one occultation moreover allows the possibility to use different bands presenting very distinctive absorption levels, therefore permitting the extraction of the CO₂ vertical profile from the top of the clouds up to 170 km high. There is also the clear possibility to probe different absorption bands originating from the different isotopologues of the CO₂. CO has been shown to act as a potential tracer of the dynamical processes occurring in the Venus atmosphere and its detection in the high-altitude range is of high interest. HCl and HF have also been detected in the SOIR spectra and vertical profiles are described. Some results will be briefly described concerning H₂O and HDO but we refer to the paper of Fedorova *et al.* [2008] for a detailed discussion. Finally the detection limits of a series of species, which have not yet been unambiguously detected, are reported and discussed.

4.1. CO₂

[27] CO₂ is the main component of the atmosphere of Venus (96.5%). The first measurements of the atmospheric composition of Venus were made by Adams and Dunham [1932] using the 100 inch reflector at Mount Wilson. They

Table 1. Possible Orders Where CO₂ Can Be Detected^a

Order	Isotopologue	Intensity	Temperature Dependence	Category
101	628	S	M	1
102	628	S	M	1
103	626 (628)	S	S	1
104	626 (628)	S	S	1
105	626 (628)	S	S	1
106	626 (628)	S	S	1
107	626	M	W	2–3
108	626	W	W	3
109	626	W	W	3
111	628	W	W	3
112	628	W	W	3
115	628	W	W	3
116	628	W	W	3
117	628	W	W	3
118	628	W	W	3
140	626	W	W	3
141	626	W	W	3
142	626	W	W	3
143	626	W	W	3
147	626	W	W	3
148	626	M	W	2–3
149	626	M	W	2–3
150	626	M	W	2–3
151	626	W	W	3
154	626	M	W	2–3
155	626	M	W	2–3
156	626	M	W	2–3
157	626	M	M	1
158	626	M	M/W	2–3
159	626	M	M	1
160	626	S	M	1
161	626	S	M	1
162	626	S	M	1
163	626	M	M	1
164	626	S	M/W	2
165	626	S	M/W	2
166	626	S	M/W	2
167	626	S	M	1
168	626	M	M	1
169	626	W	W	3
170	626	W	W	3
171	626	W	W	3

^aIndication on the altitude range probed and on the isotopologue measured. W, M, and S are for weak, medium and strong, respectively. Category is defined as the following: 1 means S/M intensity with S/M temperature dependence (cases for probing high altitudes CO₂ and temperature); 2 means S/M intensity but W temperature dependence (cases for probing high altitudes CO₂, less sensitive to temperature); 3 means M/W intensity with W temperature dependence (cases for probing lower altitudes CO₂).

discovered three bands that they tentatively attributed to CO₂. Since then, CO₂ has been proven to be the main absorber in the infrared region. Its absorption bands are present throughout the spectral domain covered by SOIR, with intensities varying over a wide range of values. Combining different spectral intervals (orders of diffraction) in which the CO₂ line strengths differ widely, the CO₂ vertical profile can be obtained from lower altitudes around 65 km to higher altitudes of about 170 km. Indeed, the interval where the CO₂ absorption is the largest will lead to information on the highest layers of the atmosphere, but will saturate for lower tangential height and, on the contrary, spectral intervals where the CO₂ lines are weaker will provide information on the deepest layers. Moreover, the choice of the spectral interval has to be done with great care, because of the high temperature dependence of some

absorption bands. This, in turn, could lead to the retrieval of temperature profiles if CO₂ bands characterized by high temperature dependency are selected. In general, a mix of intervals is chosen such that one is optimal for the CO₂ detection at high altitude, a second for CO₂ detection at lower altitudes, and finally two intervals, with higher temperature dependency, are chosen to give potential information on the temperature as a function of altitude. A summary of the possible spectral intervals and their characteristics i.e., the altitudes sounded and their temperature dependence is given in Table 1.

[28] The possibility to retrieve different isotopologues of CO₂ has already been illustrated by the discovery of the 01111–00001 band of ¹²C¹⁶O¹⁸O in the SOIR spectra [Bertaux *et al.*, 2007b; Wilquet *et al.*, 2007]. Besides this new band, ¹²C¹⁶O¹⁸O abundances can be derived from well known features around 2500 cm^{−1}. A series of occultations dedicated to the measurement of the isotopologues which can be detected by our instrument were performed during MTP 21 (orbits 583 to 598) which occurred in January 2007. The spectral region in which SOIR is active contains a large number of lines owing to the three of the four main isotopologues of CO₂. Spectral signatures of ¹²C¹⁶O¹⁶O, ¹²C¹⁶O¹⁸O, and ¹²C¹⁶O¹⁷O have been clearly identified in the SOIR spectra, as shown in Figure 6. Simultaneous measurements of the different isotopologues will lead to the determination of the ¹⁷O/¹⁶O and ¹⁸O/¹⁶O isotopic ratios as a function of altitude.

4.2. HCL and HF

[29] HCl and HF were observed for the first time in the Venus atmosphere by Connes *et al.* [1967], who estimated their mixing ratios at the cloud top as being 0.6 ppm (refined to 0.4 ± 0.07 ppm by Young [1972]) and 5 ppb, respectively. More recent nightside observations [Bézard *et al.*, 1990] provided measurements of HCl and HF below the clouds. These authors reported values of 0.5 ± 0.15 ppm and 5 ± 2 ppb, respectively, which are similar to the values found by Connes *et al.* [1967]. Preliminary measurements of Bjoraker *et al.* [1992] corresponding to altitudes above 72 km yielded a HF mixing ratio of 6.5 ± 0.3 ppb, in agreement with the values found previously. Recently, Iwagami *et al.* [2008] measured hemispheric distributions of HCl mixing ratio above and below the Venus cloud deck. These authors reported mean values of 0.76 ± 0.1 ppm at altitudes between 61 and 67 km and 0.4 ± 0.05 ppm at about 20 km. They argued that the larger HCl mixing ratio found above the clouds than that existing below the cloud requires the presence of a production process of HCl in the cloud region or above.

[30] HCl abundances are retrieved from SOIR data using a series of lines belonging to the 1–0 band in the 2905–2995 cm^{−1} spectral range (orders 130 to 133), whereas HF determination is based on two lines of the 1–0 transition (R1 and R2 at 4038.96 cm^{−1} and 4075.29 cm^{−1}, respectively, in the orders 180 and 181). The measurement points reproduced in Figure 2 correspond to occultations where one of these orders was observed. Moreover, the P3 line at 3833.66 cm^{−1} is also used to derive the HF abundance. This line, however, lies in a spectral region rich with H₂O lines which render the determination of the HF abundance less accurate.

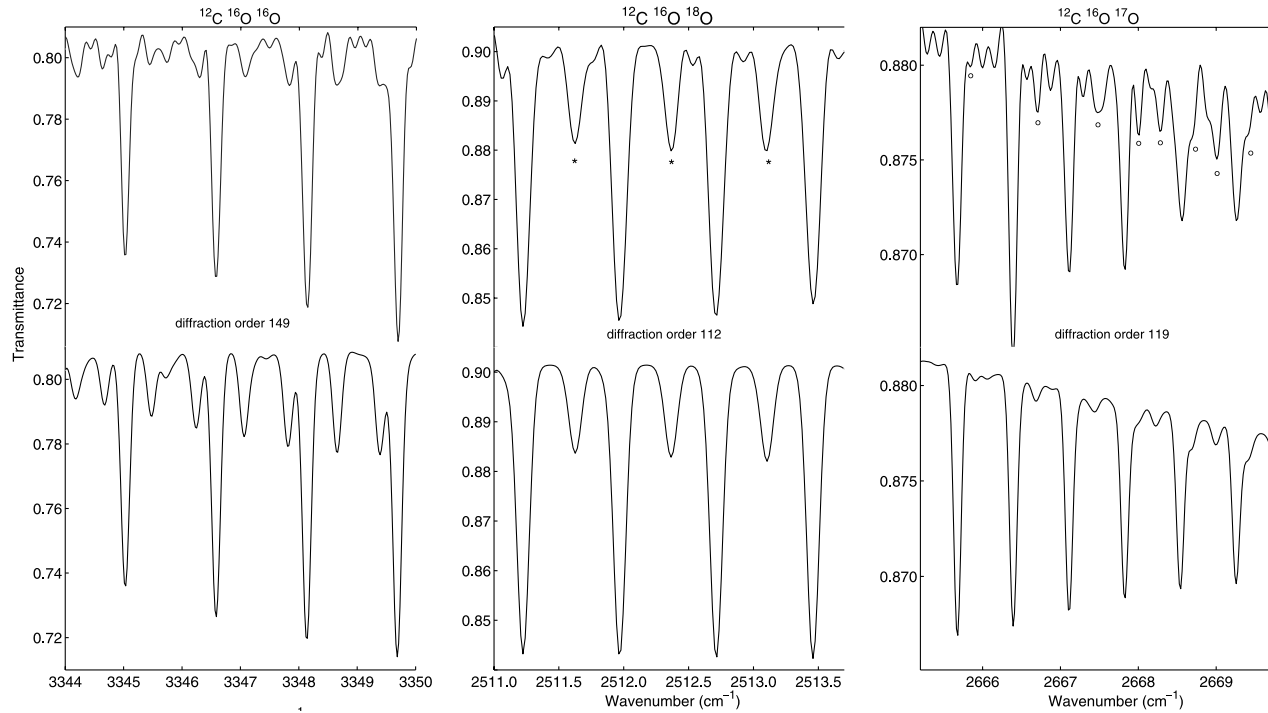


Figure 6. The isotopologues $^{12}\text{C}^{16}\text{O}^{16}\text{O}$, $^{12}\text{C}^{16}\text{O}^{18}\text{O}$, and $^{12}\text{C}^{16}\text{O}^{17}\text{O}$ have been observed during MTP 21 which was fully dedicated to the measurement of CO_2 and the determination of the $^{17}\text{O}/^{16}\text{O}$ and $^{18}\text{O}/^{16}\text{O}$ isotopic ratios as a function of altitude. Top shows observed spectra recorded by SOIR, and bottom presents the corresponding simulations. The asterisks correspond to $^{12}\text{C}^{16}\text{O}^{17}\text{O}$ lines absorbing in the same region as $^{12}\text{C}^{16}\text{O}^{18}\text{O}$, and the circles correspond to $^{12}\text{C}^{16}\text{O}^{18}\text{O}$ lines absorbing in the same region as $^{12}\text{C}^{16}\text{O}^{17}\text{O}$.

[31] Figure 7 shows some typical vertical profiles found for HCl corresponding to the orbits 341 (28 March 2007; distance to the limb at 65 km tangent height is 3346 km; 82°N), 356 (12 April 2007; distance to the limb is 3298 km; 84°N), and 366 (22 April 2007; distance to the limb is 3898 km; 73°N). The actual parameters which are retrieved are the HCl densities in each of the sounded layers and volume mixing ratios are obtained by considering the air densities calculated from pressures and temperatures given by the VENUSREF model. The HCl profiles show very similar evolution with altitude. Almost systematically we observe a depletion feature around 90 km altitude. For comparison, a profile corresponding to a constant volume mixing ratio (vmr) (0.5 ppm) is also represented. The interpretation of the depletion feature observed around 90 km is not clear. An analysis with respect to temperature has been performed, which is illustrated in Figure 8, where we have considered four different vertical profiles for the temperature: the VENUSREF model, the VENUSREF model +20% and -20%, and a more realistic profile obtained by the Vera instrument [Pätzold *et al.*, 2007]. The four corresponding density profiles are compared in Figure 8: the absolute values change, because of the temperature changes, but the depletion feature does not disappear. This would indicate that the feature is not directly temperature-dependent. We have also investigated the sensitivity of the retrieval to inaccuracies in the determination of the position of the maximum of the band pass of the AOTF function. The results, also plotted in Figure 8, show that a displace-

ment of 1.0 cm^{-1} of this maximum (the accuracy on this parameter has been estimated to be 0.83 cm^{-1}) [see Mahieux *et al.*, 2008], implies a decrease of the HCl retrieved density by 10%, but the depletion feature does not disappear.

[32] If we consider the evolution of the vmr with altitude of Figure 7, this corresponds to a more or less constant vmr comprised between 0.1 and 0.2 ppm, except around 90 km where it is slightly lower. The values at the lower boundary are somewhat lower than the values found in the literature, 0.4 ppm obtained by Connes *et al.* [1967] at an altitude of 64 km or 0.76 ppm at 61–67 km from Iwagami *et al.* [2008]. Following the interpretation proposed by Iwagami *et al.* [2008] suggesting that there should be a chemical source of HCl inside or above the clouds to explain the gradient in HCl mixing ratio that they observed, our results seem to indicate that this potential source is restricted to the cloud region.

[33] Profiles obtained in the case of HF are presented in Figure 9 for the occultations 357 (13 April 2007; distance to the limb is 3325 km; 83°N), 462 (27 July 2007; distance to the limb is 1864 km; 88°N), and 484 (18 August 2007; distance to the limb is 2670 km; 70°N). The HF abundance shows a more varying vertical distribution than HCl. Values found with SOIR seem to be in very good agreement with the values reported earlier, as for example, by Bjoraker *et al.* [1992], who measured HF abundances of 6.5 ± 0.3 ppb above 72 km. We note that both for HCl and HF, there is a

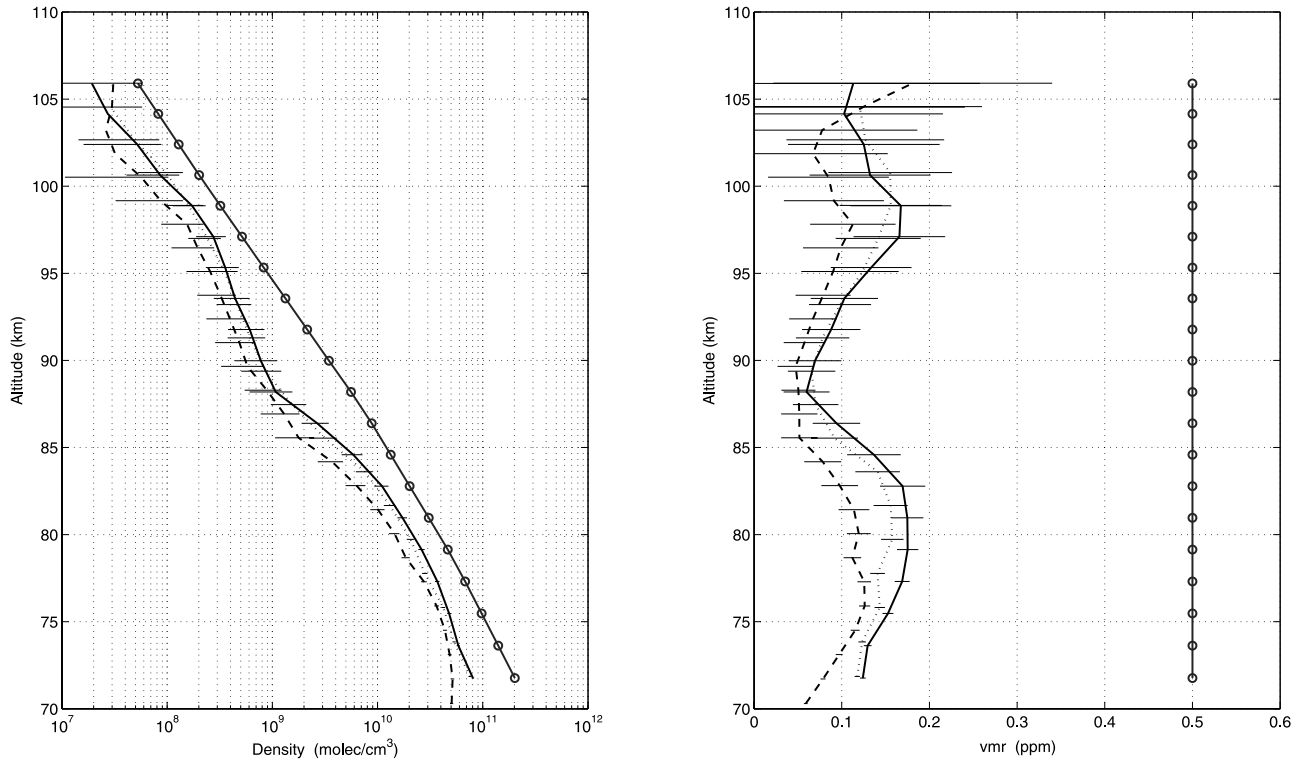


Figure 7. Vertical profiles of the HCl density (left) and volume mixing ratio in ppm (right) obtained during the three occultations 341 (solid line, 28 March 2007; distance to the limb at 65 km tangent height is 3346 km; 82°N), 356 (dotted line, 12 April 2007; distance to the limb is 3298 km; 84°N), and 366 (dashed line, 22 April 2007; distance to the limb is 3898 km; 73°N). For comparison, the solid line with dots corresponds to a profile of constant volume mixing ratio (vmr) (0.5 ppm). The vmr in this plot correspond to the ratios of the HCl densities to the total air densities obtained from the temperatures and pressures of the VENUSREF model. Error bars correspond to the fitting error on the single-fitted parameter, i.e., the density in the corresponding layer, and does not take into account the errors on the densities in the upper layers.

region of minimum vmr. However, their altitudes are different: 90 km for HCl, and 80 km for HF.

4.3. CO

[34] The primary source of CO in the atmosphere of Venus is the photodissociation of CO₂ by solar UV at altitudes higher than 120 km. The mixing ratio of CO was measured by the Pioneer Venus gas chromatograph [Oyama *et al.*, 1980] at different altitudes in the lower atmosphere (between 22 and 62 ppm at 52 km, 30 ± 18 ppm at 42 km and 20 ± 3 ppm at 22 km). The gas chromatograph on Venera 12 [Gel'man *et al.*, 1980] confirmed the low value found below 42 km (28 ± 7 ppm). Connes *et al.* [1968] reported a value of 45 ± 10 ppm at 64 km from Earth-based observations in the near-infrared. This value was corrected to 51 ± 1 ppm by Young [1972], who reanalyzed the spectra recorded by Connes *et al.* [1968]. These measurements seem to indicate the presence of a gradient in the mixing ratio of CO at least in the altitude range sounded. This was confirmed by observations of microwave lines of CO, which yielded CO mixing ratio for altitudes between 75 and 105 km. The CO mixing ratio increases from 55 ppmv at 75 km, to 130 ppmv at 85 km and 200 to 1000 ppmv at 105 km. Moreover it was shown that CO exhibits a significant diurnal variation but also strong year to year

variations [Clancy and Muhleman, 1991; Clancy *et al.*, 2003; Gurwell *et al.*, 1995]. Ground-based observations of the night side of Venus [Marcq *et al.*, 2005; Marcq *et al.*, 2006] have reported that the CO abundances in the lower atmosphere (below the clouds) showed a pronounced latitudinal enhancement of more than 10% when going toward the poles. Observations by the VIRTIS-M instrument on Venus Express [Irwin *et al.*, 2008] have shown that there was little spatial distribution of CO just above the cloud (approximately 65–70 km) at midlatitudes, with abundances of the order of 40 ± 10 ppm, with higher values at the poles, consistent with rapid downwelling bringing CO-rich air from higher altitudes.

[35] Retrieval of the vertical CO profile from SOIR spectra relies on several absorption lines of the (2–0) CO band located between 4178 cm^{-1} (order 187) and 4325 cm^{-1} (order 192). All orbits during which this spectral region is investigated are shown in Figure 2b, distinguishing orbits corresponding to low and high (>5000 km) distance to the limb. Typically the vertical profiles are obtained from 70 to 125 km altitude, as can be seen from the examples reproduced in Figure 10. Those profiles correspond to the orbits 341 (28 March 2007; distance to the limb is 3346 km; 82°N), 356 (12 April 2007; distance to the limb is 3298 km; 84°N), and 366 (22 April 2007; distance to the limb is 3898 km;

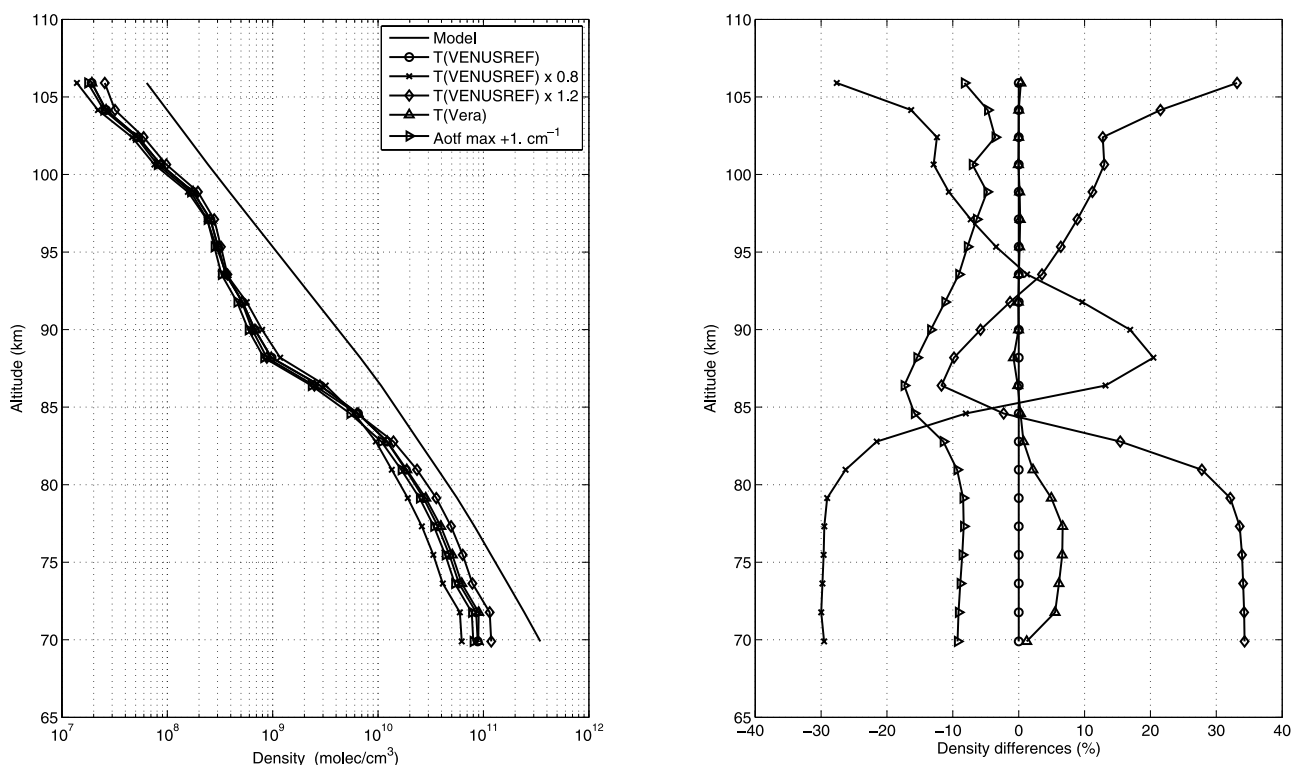


Figure 8. Investigation of the temperature effect on the detection of HCl. In the left, the corresponding density profiles are shown. For comparison, the line with dots corresponds to a profile of constant vmr of 0.5 ppm. The feature around 85 km does not disappear. In the right, the relative difference in the retrieved HCl densities is shown for the different test cases. Four different temperature profiles have been considered: VENUSREF, VENUSREF with -20% and $+20\%$ excursions, and a vertical temperature profile obtained by the Vera instrument on board Venus Express [Pätzold *et al.*, 2007]. The effect of displacing the AOTF function maximum by 1.0 cm^{-1} is also indicated.

73°N). CO vmr have been obtained from the retrieved CO densities using the air densities calculated from temperature and pressure from the VENUSREF model at the considered level. All three profiles show values for the CO vmr between 10 and 50 ppm below 90 km, and then increasing up to $4\text{--}8 \times 10^4$ ppm at 125 km, consistent with the existence of a source of CO, the photodissociation of CO_2 , at high altitudes. These profiles were obtained at the northern polar region and seem to be consistent with the observations performed by VIRTIS-M [Irwin *et al.*, 2008] which indicate high values of the CO abundance at the south pole for altitudes between 65 and 70 km. They found values ranging from 100 to 200 ppm, these values being mostly influenced by the position relative to the brightest features of the polar vortex dipole.

[36] Our value at 75 km (30 to 50 ppmv) is slightly lower than that derived from ground-based microwave (55 ppmv) by Clancy *et al.* [2003]. However, there is a major discrepancy above 75 km: our measurements show a decreasing vmr with increasing altitude, while microwave measurements indicate a steady increase. We find a minimum of CO (at 10 ppmv around 85 km). At higher altitudes, we find a steady increase of the vmr with altitude up to the limit of our measurements (4,000–8000 ppmv at 125 km). This steady exponential increase, when extrapolated upward to 140 km, would give a mixing ratio of 1, while in situ measurements with the Pioneer Venus Bus Mass Spectrometer yielded 0.4

[von Zahn *et al.*, 1980]. The increase of vmr from 90 km upward is not due to diffusive separation of CO from CO_2 , because the homopause as determined by N_2 measurements is at an altitude of 136 km. Rather, the CO gradient is dominated by the production rate of CO from CO_2 which increases with altitude. More puzzling is the strong minimum region (80–90 km) found by SOIR, which had escaped detection up to now. It should be recognized that the technique of solar occultation provides an unprecedented vertical resolution. It could be of dynamic origin or it could be the result of a strong chemical sink.

4.4. H_2O and HDO

[37] Water is scarcely present today and it is not yet known if Venus was already dry at its formation or evolved slowly to its present state. In order to refine theories and models describing the formation and evolution of Venus and its atmosphere, to characterize the escape of D atoms from the upper atmosphere and to provide a robust explanation to the problem of the origin of water on Venus, high-resolution vertically resolved measurements of H_2O and HDO and their temporal variations are needed. As illustrated in Figure 1, SOIR is able to measure both isotopologues of water simultaneously during the same occultation. Three absorption lines owing to HDO are clearly seen in the spectra recorded in the $2720\text{--}2725\text{ cm}^{-1}$ region (order 121), whereas most of the features in the $3825\text{--}3855\text{ cm}^{-1}$ region

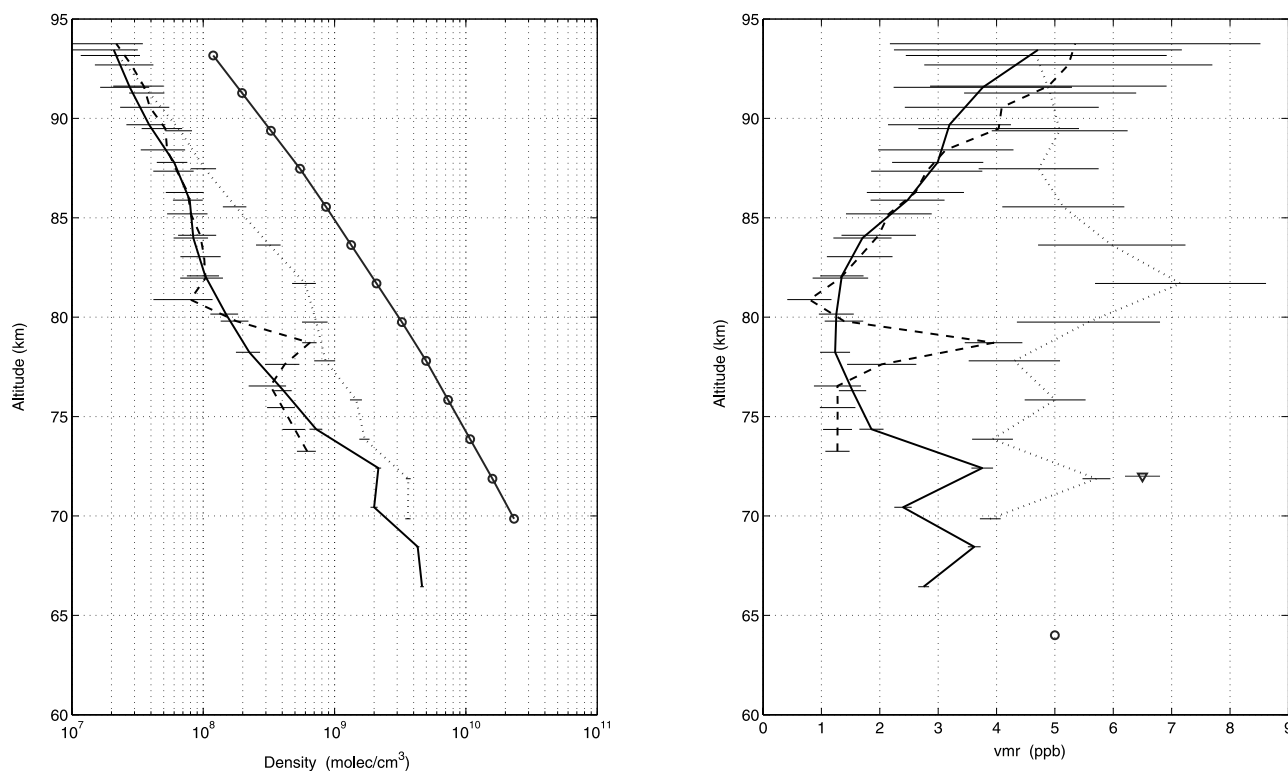


Figure 9. Vertical profiles of the HF density (left) and volume mixing ratio in ppb (right) obtained during the occultations 357 (solid line, 13 April 2007; distance to the limb at 65 km tangent height is 3325 km; 83°N), 462 (dotted line, 27 July 2007; distance to the limb is 1864 km; 88°N), and 484 (dashed line, 18 August 2007; distance to the limb is 2670 km; 70°N). For comparison, the solid line with dots corresponds to a profile of constant vmr (5 ppb). Error bars correspond to the fitting error on the single fitted parameter, i.e., the density (vmr) in the corresponding layer, and does not take into account the errors on the densities (vmr) in the upper layers. The following values from the literature are also indicated: *Connes et al.* [1967] (circles) and *Bjoraker et al.* [1992] (inverted triangles).

(order 171) originate from the main isotopologue of water H_2O and CO_2 . Such simultaneous measurements have been performed on a regular basis and are described in more detail by *Fedorova et al.* [2008].

4.5. Other Minor Constituents

[38] Spectra were recorded in different spectral intervals where some key constituents for the chemistry of the Venus atmosphere have prominent absorption features. However, some of those gases are only present as traces in the atmosphere and only upper limits of detection could be derived. As an example, OCS absorbs in the 2900–2950 cm^{-1} range, corresponding to the order 130, but spectra recorded with SOIR contain no signature of this species, as illustrated in Figure 11. The upper limit of detection for OCS has been estimated to be 1.6 ± 2 ppb between 70 and 90 km and 0.02 ± 0.01 ppm above 90 km. OCS has up to now never been observed above the cloud deck. Measurements performed at lower altitudes [*Marq et al.*, 2005; *Marq et al.*, 2006] indicate that the OCS shows latitudinal variations with abundances between 5 and 20 ppm at 30 km decreasing with altitude. At 36 km, OCS amounts to 0.55 ± 0.15 ppm. The same spectral interval could also be used to derive the upper limit of detection of H_2CO leading to the values of 3 ± 2 ppb below 90 km and 0.015 ± 0.01 ppm above 90 km.

[39] Similarly, it is also possible to determine the upper limit of other trace gases. In the case of SO_2 , the procedure is somewhat more complex since the SO_2 signature is overlapped by a band of CO_2 , as explained and discussed by *Belayev et al.* [2008], who found a positive detection of 0.3 to 3 ppmv in some occultation profiles.

4.6. Error Analysis

[40] The most critical parameters influencing the retrieval are related to the definition of the AOTF function: its formulation, the position of its maximum, and its extension in wave numbers (number of orders taken into account in the forward model). To test the sensitivity of our retrieval toward these parameters, several test cases have been investigated: (1) the function has been approximated by a sinc^2 function or by a more complex function resulting of the sum of 7 sinc^2 , with different positions of their maxima and widths; (2) the number of adjacent orders has been varied between 2 and 4; (3) the position of the function maximum has been shifted by 1.0 cm^{-1} , a slightly higher value than the estimated accuracy on the determination of this position (0.83 cm^{-1}) [*Mahieux et al.*, 2008]. The reference test case corresponds to the complex AOTF function using 3 adjacent orders (simulation on 7 orders in total), which corresponds to the normal settings used for retrieval. The results of this sensitivity study are the

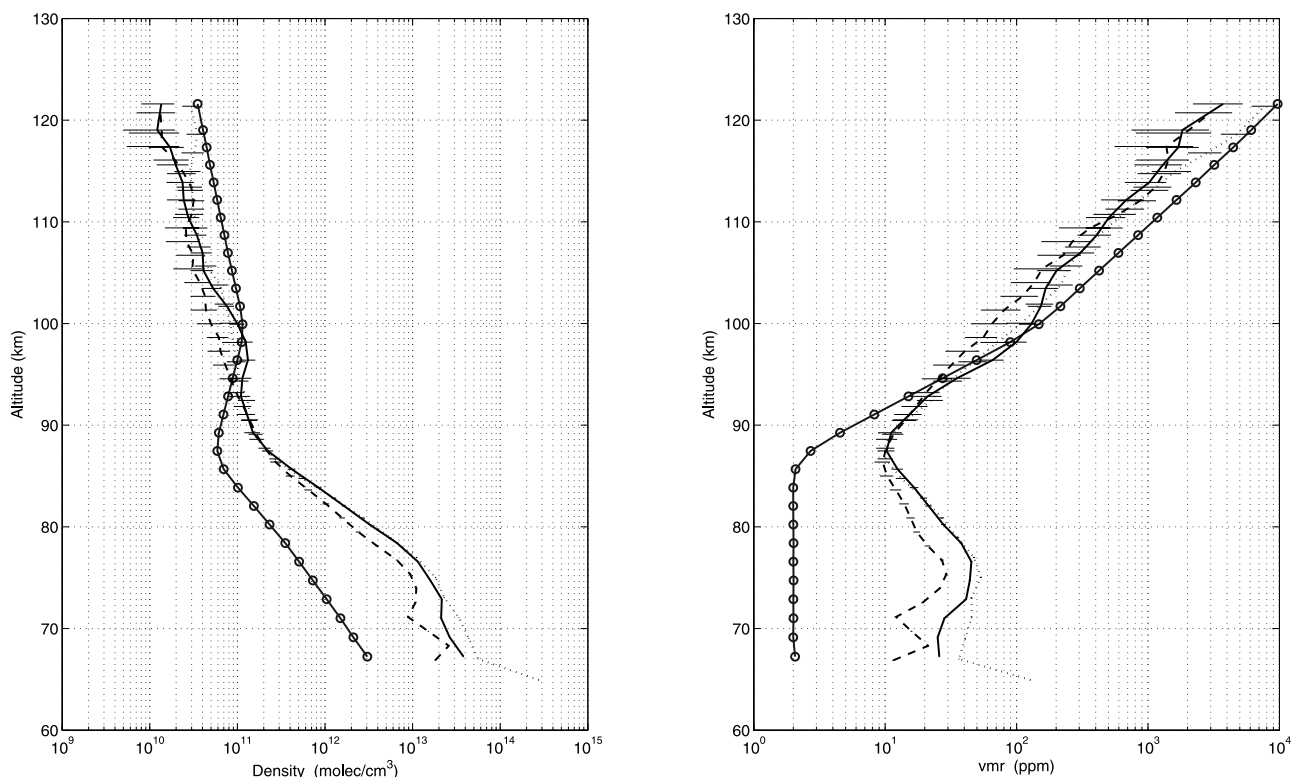


Figure 10. Vertical profiles of the CO density (left) and volume mixing ratio in ppm (right) obtained during the three occultations 341 (solid line, 28 March 2007; distance to the limb at 65 km tangent height is 3346 km; 82°N), 356 (dotted line, 12 April 2007; distance to the limb is 3298 km; 84°N), and 366 (dashed line 22 April 2007; distance to the limb is 3898 km; 73°N). For comparison, the solid line with dots corresponds to the CO in the VENUSREF model. Error bars correspond to the fitting error on the single fitted parameter, i.e., the density (vmr) in the corresponding layer, and does not take into account the errors on the densities (vmr) in the upper layers.

following: (1) choosing a sinc^2 function with 2 or 3 adjacent orders give rise to an underestimation of the CO_2 density of 20 to 50% depending on the altitude, the maximum value

being obtained at around 90 km; (2) using the complex AOTF function but on only 2 adjacent orders implies an underestimation of 5 to 40%; (3) including more adjacent

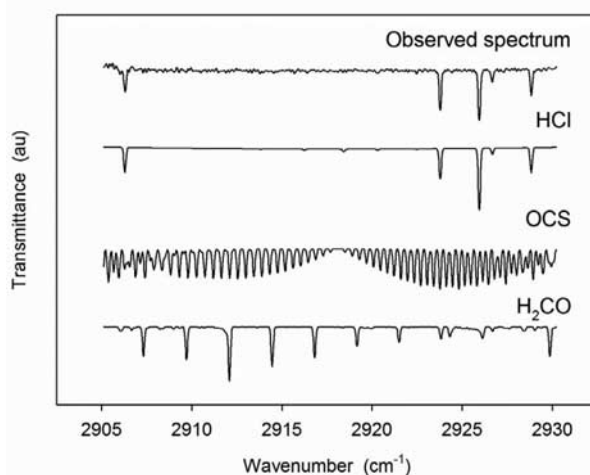


Figure 11. SOIR spectra recorded around 2915 cm^{-1} (order 130) where OCS and H_2CO signatures should be observed. The main absorption structures observed in this region are due to HCl. Absorption features due to OCS and H_2CO are also shown. From such spectra, only upper limits of detection can be derived.

orders leads to higher densities by 1–2%, but lengthens the time required for the forward modeling; (4) changing the position of the AOTF maximum implies a difference of 5 to 20%. From this discussion, it is clear that the most critical factor in the simulation or retrieval of SOIR spectra is the accurate definition of the AOTF function, in particular its width and the positions and intensities of its sidelobes. In the near future, significant efforts will be devoted to a better yet determination of these parameters from specifically dedicated in-flight calibration measurements.

5. Conclusions

[41] The SOIR spectrometer, which is part of the SPICAV/SOIR instrument on board Venus Express has proven its high potential for the detection of minor key species for the understanding of the chemical and dynamical processes occurring in the Venus mesosphere. Detection of CO, HCl, HF, H₂O, and HDO has been confirmed at altitudes ranging from 65 to 105 km, even 125 km depending on the species. Measurements have shown that the instrument was also sensitive to temperature through its observations of CO₂ absorption lines, although this will require future development of the retrieval algorithm. SOIR is also able to differentiate between three isotopologues of CO₂, namely ¹²C¹⁶O¹⁶O, ¹²C¹⁶O¹⁸O, and ¹²C¹⁶O¹⁷O. This will in fine provide the vertical distribution of the ¹⁷O/¹⁶O and ¹⁸O/¹⁶O isotopic ratios. Vertical profiles of HCl, HF, and CO in the mesosphere above the northern pole show low variability in time. The CO vertical profiles measured by SOIR indicate values of CO abundances from 10 to 50 ppm at 90 km with a pronounced minimum of 10 ppm at altitudes of the order of 85 km, followed by an increase toward the higher altitudes. HCl volume mixing ratio is about 0.1–0.2 ppm and that of HF decreases from 1 to 7 ppb showing some variability from one orbit to the other. Because of its high sensitivity and its wide spectral coverage, SOIR is also a good tool to determine upper limit of detection for a series of trace gases: for example, OCS upper limit of detection has been estimated to be 1.6 ± 2 ppb below 90 km and 0.02 ± 0.01 ppm above 90 km.

[42] **Acknowledgments.** The research program was supported by the Belgian Federal Science Policy Office and the European Space Agency (ESA, PRODEX program, contracts C 90268, 90113, and 17645). Procurement of AOTF was funded by CNES. Russian team also acknowledges RFBR grant 06-02-72563.

References

- Adams, W. S., and T. Dunham (1932), Absorption bands in the infrared spectrum of Venus, *Publ. Astron. Soc. Pac.*, **44**, 243–247, doi:10.1086/124235.
- Belyaev, D., O. Korabiev, A. Fedorova, J.-L. Bertaux, A.-C. Vandaele, F. Montmessin, A. Mahieux, V. Wilquet, and R. Drummond (2008), First observations of SO₂ above Venus' clouds by means of Solar Occultation in the Infrared, *J. Geophys. Res.*, doi:10.1029/2008JE003143, in press.
- Bertaux, J.-L., D. Nevejans, O. Korabiev, E. Villard, E. Quémerais, E. Neefs, F. Montmessin, F. Leblanc, J. P. Dubois, and E. Dimarellis (2007a), SPICAV on Venus Express: Three spectrometers to study the global structure and composition of the Venus atmosphere, *Planet. Space Sci.*, **55**, 1673–1700, doi:10.1016/j.pss.2007.01.016.
- Bertaux, J.-L., A. C. Vandaele, V. Wilquet, F. Montmessin, R. Dahoo, E. Villard, O. Korabiev, and A. Fedorova (2007b), First observation of 628 CO₂ isotopologue band at 3.3 μ m in the atmosphere of Venus by solar occultation from Venus Express, *Icarus*, **195**, 28–33, doi:10.1016/j.icarus.2008.01.001.
- Bézar, B., C. de Bergh, D. Crisp, and J. P. Maillard (1990), The deep atmosphere of Venus revealed by high-resolution nightside spectra, *Nature*, **345**, 508–511, doi:10.1038/345508a0.
- Bjoraker, G. L., H. P. Larson, M. J. Mumma, R. Timmermann, and J. L. Montani (1992), Airborne observations of the gas composition of Venus above the cloud tops: Measurements of H₂O, HDO, HF and the D/H and ¹⁸O/¹⁶O isotopic ratios, *Bull. Am. Astron. Soc.*, **24**, 995.
- Brown, L. R., C. M. Humphrey, and R. R. Gamache (2007), CO₂-broadened water in the pure rotation and ν_2 fundamental regions, *J. Mol. Spectrosc.*, **246**, 1–21, doi:10.1016/j.jms.2007.07.010.
- Clancy, R. T., and D. O. Muhleman (1991), Long-term (1979–1990) changes in the thermal, dynamical and compositional structure of the Venus mesosphere as inferred from microwave spectral line observations of ¹²CO, ¹³CO, and C¹⁸O, *Icarus*, **89**, 129–146, doi:10.1016/0019-1035(91)90093-9.
- Clancy, R. T., B. Sandor, and G. H. Moriarty-Schieven (2003), Observational definition of the Venus mesopause: Vertical structure, diurnal variation, and temporal instability, *Icarus*, **161**, 1–16, doi:10.1016/S0019-1035(02)00022-2.
- Clough, S. A., F. X. Kneizys, and R. Davies (1989), Line shape and the water vapor continuum, *Atmos. Res.*, **23**, 229–241, doi:10.1016/0169-8095(89)90020-3.
- Connes, P., J. Connes, W. S. Benedict, and L. Kaplan (1967), Traces of HCl and HF in the atmosphere of Venus, *Astrophys. J.*, **147**, 1230–1237, doi:10.1086/149124.
- Connes, P., J. Connes, L. Kaplan, and W. S. Benedict (1968), Carbon monoxide in the Venus atmosphere, *Astrophys. J.*, **152**, 731–743, doi:10.1086/149590.
- de Bergh, C., V. I. Moroz, F. W. Taylor, D. Crisp, B. Bézar, and L. V. Zasova (2006), The composition of the atmosphere of Venus below 100 km altitude: An overview, *Planet. Space Sci.*, **54**, 1389–1397, doi:10.1016/j.pss.2006.04.020.
- Fally, S., P.-F. Coheur, M. Carleer, C. Clerbaux, R. Colin, A. Jenouvrier, M.-F. Mérienne, C. Hermans, and A. C. Vandaele (2003), Water vapor line broadening and shifting by air in the 26000–13000 cm⁻¹ region, *J. Quant. Spectrosc. Radiat. Transfer*, **82**, 119–131.
- Fedorova, A., O. Korabiev, D. Belayev, A. C. Vandaele, A. Mahieux, E. Neefs, V. Wilquet, F. Montmessin, and J.-L. Bertaux (2008), HDO and H₂O vertical distribution and isotopic ratio in the Venus mesosphere by Solar Occultation at Infrared spectrometer on board Venus Express, *J. Geophys. Res.*, doi:10.1029/2008JE003146, in press.
- Fomin, B. A. (1995), Effective interpolation technique for line-by-line calculations of radiation absorption in gases, *J. Quant. Spectrosc. Radiat. Transfer*, **53**, 663–669.
- Gamache, R. R., R. L. Hawkins, and L. S. Rothman (1990), Total internal partition sums for atmospheric molecules in the temperature range 70–2005 K: Atmospheric linear molecules, *J. Mol. Spectrosc.*, **142**, 205–219, doi:10.1016/0022-2852(90)90178-S.
- Gamache, R. B., S. P. Neshyba, J.-J. Plateaux, A. Barbe, L. Régalia, and J. B. Pollack (1995), CO₂-broadening of water vapor lines, *J. Mol. Spectrosc.*, **170**, 131–151, doi:10.1006/jmsp.1995.1060.
- Gel'man, B., V. Zolotukhin, N. Lamonov, B. Levchuk, A. Lipatov, L. Mukhin, D. Nenarokov, V. Rotin, and B. Okhotnikov (1980), An analysis of the chemical composition of the atmosphere of Venus on an AMS of the Venera-12 using a gas chromatograph, *Cosmic Res., Engl. Transl.*, **17**, 585–589.
- Goody, R. M., and Y. L. Yung (1995), *Atmospheric Radiation: Theoretical Basis*, Oxford Univ. Press, New York.
- Gurwell, M., D. O. Muhleman, K. Shah, G. Berge, D. J. Rudy, and A. W. Grossman (1995), Observations of the CO bulge on Venus and implications for mesospheric winds, *Icarus*, **115**, 141–158, doi:10.1006/icar.1995.1085.
- Hedin, A. E., H. B. Niemann, and W. T. Kasprzak (1983), Global empirical model of the Venus thermosphere, *J. Geophys. Res.*, **88**, 73–83, doi:10.1029/JA088iA01p00073.
- Irwin, P. G. J., R. de Kok, A. Negrão, C. C. C. Tsang, C. F. Wilson, P. Drossart, G. Piccioni, D. Grassi, and F. W. Taylor (2008), Spatial variability of carbon monoxide in Venus' mesosphere from Venus Express/Visible and Infrared Thermal Imaging Spectrometer measurements, *J. Geophys. Res.*, **113**, E00B01, doi:10.1029/2008JE003093.
- Iwagami, N., et al. (2008), Hemispheric distributions of HCl above and below the Venus' clouds by ground-based 1.7 μ m spectroscopy, *Planet. Space Sci.*, **56**, 1424–1434.
- Jenouvrier, A., L. Daumont, L. Régalia-Jarlot, V. G. Tyuterev, M. Carleer, A. C. Vandaele, S. Mikhailenko, and S. Fally (2007), Fourier transform measurements of water vapor line parameters in the 4200–6600 cm⁻¹ region, *J. Mol. Spectrosc.*, **105**, 326–355.
- Mahieux, A., et al. (2008), In-flight performance and calibration of SPICAV SOIR on board Venus Express, *Appl. Opt.*, **47**(13), 2252–2265, doi:10.1364/AO.47.002252.

- Marcq, E., B. Bézard, T. Encrenaz, and M. Birlan (2005), Latitudinal variations of CO and OCS in the lower atmosphere of Venus from near-infrared nightside spectro-imaging, *Icarus*, *179*, 375–386, doi:10.1016/j.icarus.2005.06.018.
- Marcq, E., T. Encrenaz, B. Bézard, and M. Birlan (2006), Remote sensing of Venus' lower atmosphere from ground-based IR spectroscopy: Latitudinal and vertical distribution of minor species, *Planet. Space Sci.*, *54*, 1360–1370, doi:10.1016/j.pss.2006.04.024.
- Mérienne, M.-F., A. Jenouvrier, C. Hermans, A. C. Vandaele, M. Carleer, C. Clerbaux, P.-F. Coheur, R. Colin, S. Fally, and M. Bach (2003), Water vapor line parameters in the 13000–9250 cm^{-1} region, *J. Quant. Spectrosc. Radiat. Transfer*, *82*, 99–118.
- Mueller-Wodarg, I., and S. Tingle (2008), Vertical structure above the clouds: Towards a unified model, paper presented at XLIII Rencontres de Moriond, Venus Express Scientific Workshop, Eur. Space Agency, La Thuile, Italy, 3–7 Mar.
- Nevejans, D., et al. (2006), Compact high-resolution space-borne echelle grating spectrometer with AOTF based on order sorting for the infrared domain from 2.2 to 4.3 micrometer, *Appl. Opt.*, *45*(21), 5191–5206, doi:10.1364/AO.45.005191.
- Oyama, V., G. Carle, F. Woeller, J. B. Pollack, R. Reynolds, and R. Craig (1980), Pioneer Venus gas chromatography of the lower atmosphere of Venus, *J. Geophys. Res.*, *85*, 7891–7902, doi:10.1029/JA085iA13p07891.
- Pätzold, M., et al. (2007), The structure of Venus' middle atmosphere and ionosphere, *Nature*, *450*, 657–660, doi:10.1038/nature06239.
- Pollack, J. B., et al. (1993), Near-infrared light from Venus' nightside: A spectroscopic analysis, *Icarus*, *103*, 1–42, doi:10.1006/icar.1993.1055.
- Rothman, L. S., et al. (2005), The HITRAN 2005 molecular spectroscopic database, *J. Quant. Spectrosc. Radiat. Transfer*, *96*, 139–204.
- Seiff, A., J. T. Schofield, A. Kliore, F. W. Taylor, S. S. Limaye, H. E. Revercomb, L. A. Sromovsky, V. V. Kerzhanovich, V. I. Moroz, and M. Y. Marov (1985), Models of the structure of the atmosphere of Venus from the surface to 100 kilometers altitude, *Adv. Space Res.*, *5*(11), 3–58, doi:10.1016/0273-1177(85)90197-8.
- Sung, K., and P. Varanasi (2005), CO₂-broadened half-widths and CO₂-induced line shifts of ¹²C¹⁶O relevant to the atmospheric spectra of Venus and Mars, *J. Quant. Spectrosc. Radiat. Transfer*, *91*, 319–322, doi:10.1016/j.jqsrt.2004.05.063.
- Titov, D. V., et al. (2006), Venus Express science planning, *Planet. Space Sci.*, *54*, 1279–1297, doi:10.1016/j.pss.2006.04.017.
- Toth, R. A., and L. A. Darnton (1974), Linewidths of HCl broadened by CO₂ and N₂ and CO broadened by CO₂, *J. Mol. Spectrosc.*, *49*, 100–105, doi:10.1016/0022-2852(74)90099-X.
- Vandaele, A. C., M. Kruglanski, and M. De Mazière (2006), Simulation and retrieval of atmospheric spectra using ASIMUT, paper presented at Atmospheric Science Conference, Eur. Space Agency, Frascati, Italy.
- von Zahn, U., K. H. Fricke, D. M. Hunten, D. Krankowsky, K. Mauersberger, and A. O. Nier (1980), The upper atmosphere of Venus during morning conditions, *J. Geophys. Res.*, *85*, 7829–7840, doi:10.1029/JA085iA13p07829.
- Wilquet, V., A. Mahieux, A. C. Vandaele, V. Perevalov, S. Tashkun, A. Fedorova, O. Korablev, F. Montmessin, R. Dahoo, and J.-L. Bertaux (2007), Line parameters for the 01111–00001 band of ¹²C¹⁶O¹⁸O from SOIR measurements of the Venus atmosphere, *J. Quant. Spectrosc. Radiat. Transfer*, *109*, 895–905.
- Young, L. (1972), High resolution spectra of Venus: A review, *Icarus*, *17*, 632–658, doi:10.1016/0019-1035(72)90029-2.
- D. Belyaev, A. Fedorova, and O. Korablev, Space Research Institute, 84/32 Profsoyuznaya Street., 117997, Moscow, Russia.
- J.-L. Bertaux and F. Montmessin, Service d'Aéronomie du CNRS, BP3, 91371, Verrières-le-Buisson, France.
- R. Drummond, A. Mahieux, M. De Mazière, E. Neefs, A. C. Vandaele, and V. Wilquet, Belgian Institute for Space Aeronomy, 3 avenue Circulaire, B-1180 Brussels, Belgium. (a-c.vandaele@aeronomie.be)